agronomy

MDPI

Article

Multi-Level Data Integration Decodes the Metabolic Strategies of Kawisari Coffee Hybrid Resistance to *Hemileia vastatrix*

Leonor Guerra-Guimarães [1,*], Jéfyne Campos Carréra [1,2], Carla Pinheiro [3,4,*], Martim De Freitas [1,3], Henrique Costa [1], Manzur-E-Mohsina Ferdous [5], Thomas Roitsch [6,7], Deila Magda dos Santos Botelho [8], Helena Gil Azinheira [1], John Charles D'Auria [9] and Maria do Céu Silva [1]

[1] CIFC—Centro de Investigação das Ferrugens do Cafeeiro, LEAF—Linking Landscape, Environment, Agriculture and Food Research Unit, TERRA Associate Laboratory, Instituto Superior de Agronomia, Universidade de Lisboa, Tapada da Ajuda, 1349-017 Lisboa, Portugal; jefynecarrera@gmail.com (J.C.C.); m.gordinho@campus.fct.unl.pt (M.D.F.)
[2] Instituto de Ciências Naturais (ICN), Departamento de Biologia, Universidade Federal de Lavras (UFLA), Lavras 37203-202, Brazil
[3] UCIBIO Applied Molecular Biosciences Unit, Department of Life Sciences, NOVA School of Science and Technology, Universidade NOVA de Lisboa, 2829-516 Caparica, Portugal
[4] Associate Laboratory i4HB Institute for Health and Bioeconomy, NOVA School of Science and Technology, Universidade NOVA de Lisboa, 2829-516 Caparica, Portugal
[5] Department of Plant and Environmental Sciences, Section for Crop Sciences, Copenhagen University, Højbakkegård Allé 13, 2630 Taastrup, Denmark
[6] Department of Environmental Sciences, Aarhus University, Frederiksborgvej 399, 2630 Roskilde, Denmark
[7] Global Change Research Institute CAS, CzechGlobe, Bělidla 986/4a, 603 00 Brno, Czech Republic
[8] Departamento de Fitopatologia, Universidade Federal de Lavras (UFLA), Lavras 37203-202, Brazil
[9] Research Group Metabolic Diversity, Department of Molecular Genetics, Leibniz Institute of Plant Genetics and Crop Plant Research (IPK Gatersleben), OT Gatersleben, Corrensstraße 3, 06466 Seeland, Germany; dauria@ipk-gatersleben.de
* Correspondence: leonorguimaraes@edu.ulisboa.pt (L.G.-G.); cm.pinheiro@fct.unl.pt (C.P.)

Abstract

Plants have developed mechanisms to regulate carbon metabolism during growth and development under both optimal and stressful conditions. In the biotrophic interaction between *Coffea* spp. and *Hemileia vastatrix*, the plant restricts pathogen access to nutrients, whereas the fungus attempts to manipulate host metabolism. Here, we investigate the metabolic mechanisms underlying post-haustorial resistance of the Kawisari coffee hybrid to *H. vastatrix* by integrating metabolomic, starch, enzymatic, and gene expression analyses to distinguish resistant (R) from susceptible (S) responses. Polar untargeted metabolomics (GC-TOF-MS) revealed distinct modulation of sugars, amino acids, polyamines, and phenolics between R and S responses. Combining these metabolomic profiles with starch quantification, semi-high-throughput enzyme activity assays, and RT-qPCR gene expression analysis revealed a distinct pattern of carbon reallocation in the resistant response. Specifically, resistance was associated with an early (4 DAI) transcriptional activation of the pentose phosphate pathway, evidenced by the significant upregulation of *RPE* (ribulose-phosphate 3-epimerase) and *TK* (transketolase), supporting the generation of reducing power and precursor skeletons for phenolic defenses (such as caffeoylquinic acids, salicylic acid, and flavonoids). This was coordinated with elevated activity of cytosolic/vacuolar invertases (cytInv, vacInv) and phosphoglucomutase (PGM) at later stages (7–16 DAI), consistent with the regulation of starch utilization and nitrogen remobilization, involving L-asparagine, L-ornithine, and spermine. These findings underscore the pivotal role of primary metabolic networks in supporting resistance to *H. vastatrix* and

Academic Editor: Imre J. Holb

Received: 28 September 2026
Revised: 24 October 2026
Accepted: 26 October 2026
Published: 4 November 2026

Copyright: © 2026 by the authors. Licensee MDPI, Basel, Switzerland. This article is an open access article distributed under the terms and conditions of the Creative Commons Attribution (CC BY) license.

identify promising biochemical targets for breeding coffee cultivars with enhanced resistance to rust under climate change scenarios.

Keywords: coffee leaf rust (CLR); GC-TOF-MS polar untargeted metabolomics; primary metabolism restructuring; semi-high throughput enzyme activity; gene expression (RT-qPCR)

1. Introduction

Coffee leaf rust (CLR), caused by the biotrophic fungus *Hemileia vastatrix*, remains one of the most severe threats to *Coffea arabica*, which accounts for nearly 60% of global coffee production [1,2]. By infecting leaves, *H. vastatrix* disrupts photosynthesis, leading to defoliation, reduced yields, and, in severe cases, plant death [3]. The disease spreads rapidly in warm and humid environments. Although resistant varieties, fungicides, and improved agricultural practices are commonly used for control, disease management is continuously challenged by evolving fungal strains and climate change [1,3,4].

Achieving effective, stable, and broad-spectrum resistance in coffee varieties remains a major challenge [4,5]. Traditionally, selection for resistance against *H. vastatrix* has relied on major resistance genes/factors (S_H1–S_H9), derived from inter- and intra-species *Coffea* crosses, following the recognition of the 'gene-for-gene' concept in coffee–rust interactions [6]. Beyond S_H1–S_H9, additional resistance genes have been reported to contribute to resistance against more than 55 physiological races of *H. vastatrix*, although they require further characterization [1,7–9]. One promising genetic resource for enhancing CLR resistance is the Kawisari hybrid (*Coffea arabica* × *Coffea liberica*), which has been incorporated into breeding programs in India to enhance the resilience of *C. arabica* [6,10]. This hybrid combines the high cup quality of *C. arabica* [11–13] with the natural disease resistance of *C. liberica* [10,14,15]. Although this hybrid has shown great potential for disease resistance, the underlying molecular and biochemical networks that orchestrate its defense response have yet to be fully elucidated.

Plant immunity is an energy-demanding process that requires profound metabolic restructuring, shifting resources from growth to defense through the tight regulation of carbon and nitrogen pathways [16–18]. Accumulating evidence from several plant–pathogen systems indicates that this primary metabolic shift is instrumental in sustaining active host responses. For instance, the activation of the pentose phosphate pathway (PPP) in the cytosol provides critical reducing power (NADPH) through its irreversible oxidative steps to drive defense-related ROS production [19], whereas its reversible reactions equilibrate the hexose-P/triose-P pool to supply erythrose-4-phosphate precursors necessary for downstream aromatic amino acid and phenolic biosynthesis, including cell wall lignification [20]. Concurrently, the mobilization of nitrogen-derived compounds, such as specific amino acid pools and polyamines, acts as a pivotal signaling mechanism and metabolic buffer during fungal attack [21,22].

In biotrophic interactions, such as coffee leaf rust, managing primary resources is critical, as the host attempts to restrict fungal access to essential sugars, while *H. vastatrix* employs strategies to manipulate coffee metabolism to its advantage, thereby dictating infection success [1,23]. Previous proteomics studies of *C. arabica* leaves infected with *H. vastatrix* have revealed significant changes in proteins involved in photosynthesis, primary metabolism, and redox homeostasis, which may contribute to the mitigation of oxidative stress and the reinforcement of structural barriers [24,25]. Cytological studies have linked the post-haustorial resistance of the Kawisari hybrid to an early hypersensitive response (HR), accumulation of phenolic compounds, and haustorium encasement with

callose [26,27]. In parallel, our prior transcriptomic profiling (RNA-Seq using the Illumina NovaSeq platform) of this exact biological system revealed major transcriptional reprogramming, particularly targeting carbon and energy metabolism-related pathways during infection [27]. Building upon these findings, the present study was designed to achieve a multi-level functional validation of selected transcriptomic signatures. Specifically, we aimed to determine how those underlying transcriptional shifts are reflected in metabolic profiles, dynamic carbon partitioning (starch and soluble sugars), and enzymatic activity patterns during infection. This functional integration is increasingly important in the context of climate change, as drought, heat, and other abiotic stresses compromise primary productivity and carbon availability, intensifying the trade-off between growth and defence, and potentially reducing the plant's capacity to effectively build up resistance against *H. vastatrix* [28–30].

To gain a comprehensive understanding of the biochemical shifts during *H. vastatrix* infection, we conducted a multi-level analysis integrating untargeted metabolomics (sugars, amino acids, and organic acids), starch quantification, enzymatic activity profiling [31], and gene expression profiling of Kawisari hybrid leaf samples. By applying a data integration approach, we aimed to identify the core metabolic signatures and defense-associated pathways that distinguish resistant from susceptible responses. These findings will enhance our understanding of how primary metabolic networks sustain CLR resistance and provide valuable targets for breeding or biotechnological interventions, ultimately supporting sustainable coffee production in disease-prone regions.

2. Material and Methods

2.1. Biological Material and Inoculation

Fifteen-year-old clonally propagated stem cuttings of the Kawisari hybrid (*C. arabica* × *C. liberica*), a coffee genotype used as a donor for resistance in Arabica breeding programs in India, were grown in 50 L pots containing a soil:peat:sand (1:1:1) mixture under greenhouse conditions (90% air humidity and an average temperature of 22 °C). Two *Hemileia vastatrix* races from the CIFC collection were used in this study: race XIII, which establishes a compatible interaction (susceptible reaction) characterized by fungal growth and plant disease symptoms, and race II, which establishes an incompatible interaction (resistance reaction) characterized by resistant symptoms and fungal death [1]. Fresh uredospores of *H. vastatrix* (1 mg/pair of leaves) were spread on the lower surface of young coffee leaves, following Silva et al. [32]. Mock-inoculated leaves (sprayed only with water) were used as controls. Leaves were collected at 1, 4, 7 and 16 days after inoculation (DAI) for experimental purposes. All collected leaves (with excised midribs) were immediately frozen in liquid nitrogen and preserved at −80 °C until use. For each condition and time point, five biological replicates were analyzed ($N = 5$), with each replicate corresponding to one pair of leaves collected from five individual clonal plants maintained throughout the experiment.

2.2. Polar-Untargeted Metabolic Analysis by GC-TOF-MS

The frozen leaf samples were ground into powder using liquid nitrogen and preserved at −80 °C until required. Polar metabolites were extracted from 50 mg of ground leaf material in 2 mL microtubes, with five replicates for each sample. Extraction was performed using 1.5 mL of a solvent mixture of methyl-tert-butyl-ether:methanol (MTBE:MeOH, 3:1, *v:v*) containing the internal standard L-alanine-d4 (50 µL/100 mL), as described by Salem et al. [33]. Briefly, the microtubes were vortexed and incubated on an orbital shaker (40 rpm) for 45 min at 4 °C, followed by a 15 min sonication in a 4 °C water bath. The samples were centrifuged at 10,000× *g* for 10 min at 4 °C. From the upper solvent

phase, 0.5 mL aliquots were transferred into new microtubes and dried in a speed vacuum for 45 min for subsequent GC-TOF-MS analysis of polar metabolites. The insoluble pellet was washed multiple times and used to determine starch content.

Metabolite profiling was performed according to the protocol adapted for coffee leaf matrices described by Carrera et al. [34]. Samples were analyzed in splitless mode using a LECO Pegasus HT time-of-flight mass spectrometer (LECO, St. Joseph, MI, USA) hyphenated with an Agilent 7890 gas chromatograph and an Agilent DB-35MS capillary column (30 m × 0.25 mm × 0.25 µm). The identification of metabolic features, determination of peak intensities, and normalization were performed as described by Carréra et al. [34].

All metabolic class identifications were manually validated using the GOLM, KEGG, and HMDB metabolite databases [35–37]. After annotating the metabolic classes, 175 metabolic features were excluded from the subsequent analysis. These features included reagents (52), unknown features (8), and features that were not clearly identified as plant metabolites (115).

2.3. Starch Quantification

Pellets obtained from the metabolic extraction, and according to Salem et al. [33], were washed several times, first with methanol, then with a washing buffer (30 mM Tris-HCl pH 8.8, 7 M urea, 2 M thiourea, 15 mM DTT, 4% CHAPS), and finally with 70% ethanol (at least twice). Once the pellets were completely dry, 0.4 mL of a 0.7% aqueous α-amylase solution (Sigma-Aldrich, A4582, St. Louis, MO, USA) was added to each tube, following Pinheiro et al. [38]. The tubes were boiled for 3 min, and the starch was gelatinized by heating at 120 °C for 50 min (the tubes were pierced and covered with aluminum foil before autoclaving). After cooling to room temperature, 0.6 mL of an amyloglucosidase (Sigma-Aldrich A7420) solution (prepared with 1 M acetate buffer pH 4.8 and 1.67 mg/mL of amyloglucosidase) was added to the tubes, which were then incubated at 60 °C for 2 h with agitation. After centrifugation at 12,000× *g* for 5 min, the supernatant (containing hydrolysed glucose) was used to quantify starch (as glucose equivalents) using the ®R-BIOPHARM Starch Kit (Darmstadt, Germany), as modified by Pinheiro et al. [38]. Glucose solutions ranging from 0–1.4 gL^{-1} were used as standards, with absorbance readings taken at 490 nm. Results are presented as mmol glucose equivalents per gram of fresh weight (FW). As a positive control, five replicates of 10 mg of commercial starch were processed in the same manner as the biological samples.

2.4. Protein Extraction

Protein extraction was performed using 200 mg of ground leaf material preserved at −80 °C (five replicates per sample). The protein fractionation extraction method described by Jammer et al. [39] was employed with some modifications. Briefly, extraction was carried out using 1.5 mL of 100 mM potassium phosphate buffer, pH 7.4, containing 7.5 mM $MgCl_2$, 20 µM $MnCl_2$, 10% glycerol, 5 mM DTT, 5 mM ascorbic acid, and 1.5% sodium sulphite. Extraction buffer (1.5 mL) and 25% PVPP (*w*/*w*) were added to the plant material. The mixture was incubated for 40 min in a head-to-head shaker at 25 rpm at 4 °C, then centrifuged twice for 10 min at 13,500× *g* at 4 °C to obtain a clear supernatant. The supernatants were dialyzed overnight in cellulose membranes (12,000 Da) using 20 mM potassium phosphate buffer pH 7.4 at 4 °C and stored at −20 °C before being used for intracellular enzyme activity assays.

The cell wall (CW) proteins retained in the pellet were extracted. The pellets were washed thrice with 1 mL of distilled water and centrifuged for 10 min at 10,000× *g* at 4 °C. The washed pellets were then extracted with 1 mL of a salt buffer containing 40 mM Tris-HCl pH 7.6, 3 mM $MgCl_2$, 1 mM EDTA, and 1 M NaCl, incubated overnight at 4 °C in the head-to-head shaker. The mixture was centrifuged twice for 10 min at 13,500× *g* at 4 °C,

and the resulting supernatant was dialyzed following the previously mentioned procedure. These CW protein extracts were stored at −20 °C prior to use in CW invertase and CW peroxidase assays.

2.5. Enzyme Activity Assays

All kinetic enzyme activity assays were performed using a 96-well microtiter plate setup optimized for semi-high-throughput applications [31]. For each assay, 25 µL aliquots of protein extracts were used in a total reaction volume of 160 µL. The plates were incubated at 30 °C for 40 min in a plate reader (Ascent Multiskan; Thermo Fisher Scientific, Waltham, MA, USA). The buffer mixture components for aldolase (Ald; EC 4.1.2.13), phosphoglucomutase (PGM; EC 5.4.2.2), phosphoglucose isomerase (PGI; EC 5.3.1.9), glucose-6-phosphate dehydrogenase (G6PDH; EC 1.1.1.49), and UDP-glucose pyrophosphorylase (UGPase; EC 2.7.7.9) were based on the protocols described by Jammer et al. [39], with absorbance recorded at 340 nm. For cell wall peroxidase (POX; EC 1.11.1.7), the buffer components were prepared as in [40], with absorbance measured at 450 nm. In contrast to the kinetic assays, the activity of invertases (Inv; EC 3.2.1.26), including cell wall (cw), vacuolar (vac), and cytoplasmic (cyt) isoforms, was measured using an end-point assay based on Jammer et al. [39], with absorbance recorded at 405 nm. All enzymatic activities were normalized to protein content (nkat mg protein^{-1}), determined using the Bradford assay [41], following the Bio-Rad protocol for microtiter plates, according to the manufacturer's guidelines. Bovine serum albumin (BSA) was used as the standard, and absorbance readings were obtained at 595 nm.

2.6. RNA Extraction and cDNA Synthesis

Total RNA was extracted from frozen coffee leaf samples using the Spectrum™ Plant Total RNA Kit (Sigma-Aldrich, USA), with in-column DNase I digestion, according to the manufacturer's instructions. RNA purity was assessed by electrophoresis on 1.2% agarose gels, and the concentration was calculated from measurements at 260/280 nm and 260/230 nm using a spectrophotometer (NanoDrop 1000, Thermo Fisher Scientific). First-strand cDNA was synthesized from 1 µg of total RNA in 20 µL final volume, using RevertAid1H Minus Reverse Transcriptase (Fermentas, Burlington, ON, Canada) anchored with Oligo(dT) 18primer (STAB VIDA, Caparica, Portugal), according to the manufacturer's instructions.

2.7. Quantitative Real-Time qPCR

To complement our untargeted metabolomic profiling and enzyme activity assays, we investigated whether the primary metabolic shifts observed during *H. vastatrix* infection were associated with changes in the expression of genes involved in central carbon metabolism. Based on candidate genes previously identified through transcriptomic profiling of the Kawisari hybrid–*H. vastatrix* interaction [27], eight genes encoding key enzymes at critical branch points connecting carbon partitioning, the pentose phosphate pathway, and secondary metabolism were selected for RT-qPCR analysis. These included ribulose-phosphate 3-epimerase (*RPE*; EC 5.1.3.1), phosphoribulokinase (*PRK*; EC 2.7.1.19), hydroxypyruvate reductase (*HPR*; EC 1.1.1.81), fructose-bisphosphatase (*FBP*; EC 3.1.3.11), fructose-bisphosphate aldolase (*FBAase*; EC 4.1.2.13), sorbitol-6-phosphate dehydrogenase (*S6PDH*; EC 1.1.1.200), pyruvate, phosphate dikinase (*PPDK*; EC 2.7.9.1), and transketolase (*TK*; EC 2.2.1.1). Quantitative PCR (RT-qPCR) was performed using SYBR Green Supermix (Bio-Rad) in a CFX Real-Time qPCR Detection System (Bio-Rad, Hercules, CA, USA). Each 15 µL reaction comprised 5 µL cDNA template (2.5 ng/µL), 7.5 µL SYBR Green Supermix (Bio-Rad, USA), and 0.45 µL of each primer (10 µM). Thermal cycling started with a denaturation step at 95 °C for 3 min, followed by 45 cycles of

denaturation at 95 °C for 15 s and annealing at the respective temperature for each gene for 30 s (Supplementary Table S1). Each set of reactions included a negative control without a template. Melting curve analysis was performed at the end of the RT-qPCR cycles, from the annealing temperature to 95 °C, with the temperature increasing stepwise by 0.5 °C every 10 s. Each PCR reaction was performed in duplicate, and amplicon specificity was checked by melting curve analysis and 3% agarose gel electrophoresis. *Actin-11* (Act) and *polyubiquitin-like* (Ubq) were used as reference genes, and gene expression was calculated according to Tavares et al. [42]. All primers were designed using PerlPrimer v1.1.21 Copyright © 2003–2011 Owen Marshall (Supplementary Table S1).

2.8. Data Analysis

Due to incomplete trimethylsilylation of primary amines and silylation state fluctuations, several unique biological metabolites yielded multiple chromatographic peaks representing different silylation or isomeric states (such as asparagine 3TMS and 4TMS) [43]. These split rows were mathematically consolidated by summing the peak heights of their respective silylation products and isomers (such as *syn* and *anti*-conformers of methoximated sugars) for each sample [43,44]. This consolidated matrix was utilized as the final input for downstream multivariate statistical analyses. Metabolic classes were analyzed using Microsoft Office Excel (Microsoft Corp., Redmond, WA, USA) and R software [45]. Venn diagrams were generated using the web tool provided by the Bioinformatics & Evolutionary Genomics group at Ghent University (http://bioinformatics.psb.ugent.be/webtools/Venn/, accessed on 13 September 2026). Multivariate and pathway analyses were conducted using MetaboAnalyst 6.0 [46]. In MetaboAnalyst, the metabolites with constant or single values across samples were excluded from the statistical analysis. Additionally, metabolites with more than 50% missing values were removed, and for the remaining metabolites, missing values were imputed with 1/5 of the minimum positive value for each variable. All data were log10-transformed and mean-centered prior to analysis.

To assess the variations among the control, resistant, and susceptible samples at each time point, principal component analysis (PCA) coupled with permutational multivariate analysis of variance (PERMANOVA) was conducted on the metabolic data. Metabolic pathway analysis was conducted using the names of the metabolites as inputs. Pathway enrichment was assessed using Fisher's exact test (significance level of $\alpha = 0.05$) and the *Arabidopsis thaliana* metabolome from the KEGG database [36] as the reference.

Differences in starch content among the control, resistant, and susceptible samples were analyzed using one-way analysis of variance (ANOVA), followed by post hoc pairwise comparisons with Tukey's Honestly Significant Difference (HSD) test. Differential gene expression between resistant and susceptible samples was assessed using Student's *t*-test, with Welch's correction applied when the assumption of homogeneity of variance was violated. Statistical significance was set at $\alpha = 0.05$. Both analyses were conducted using R (version 4.3.1; R Core Team, 2023) with the following packages: *circlize* [47], *ComplexHeatmap* [48,49], *dplyr* [50], *ggplot2* [51], *pacman* [52], *car* [53], *RVAideMemoire* [54], and *vip* [55].

Additionally, partial least squares discriminant analysis (PLS-DA) was applied to the integrated dataset, incorporating primary metabolism-related metabolites, starch content, enzymatic activities, and gene expression profiles. The model performance was evaluated via 5-fold cross-validation across up to five components using three classification accuracy metrics. Key variables driving group separation were identified based on variable importance in projection scores, with a selection threshold of VIP > 1.5.

3. Results

3.1. Non-Targeted Metabolic Analysis by GC-TOF-MS

Non-targeted metabolomic analysis using GC-TOF-MS detected approximately 581 metabolic features in the leaves of the Kawisari hybrid across all samples [control (C), resistant (R), and susceptible (S)] and time points (1, 4, 7, and 16 days after inoculation with *H. vastatrix*). To assess metabolic modulation during infection, the metabolite profiles were compared across samples at each time point. This analysis identified 33, 81, 63, and 38 significantly different metabolites at 1, 4, 7, and 16 DAI, respectively, for a total of 215 (Figure 1A and Supplementary Table S2). These significantly different metabolites were categorized into metabolic classes using annotations from the Golm Metabolome and KEGG databases. Sugars and amino acids consistently represented the largest categories (≈50% at each time point), followed by phenylpropanoids, phenolics, other organic acids, lipids, amines and alkaloids (Figure 1A). The overall distribution of metabolic classes remained relatively stable across time points. The Venn diagram revealed that several metabolites were shared across multiple time points, with piperidine-2-carboxylic acid, cytidine, L-ornithine, trehalose, L-asparagine, sophorose, and N-acetyl-galactosamine consistently detected in all samples and at all time points (Figure 1B). After removing duplicates, 128 unique metabolites were obtained from the 215.

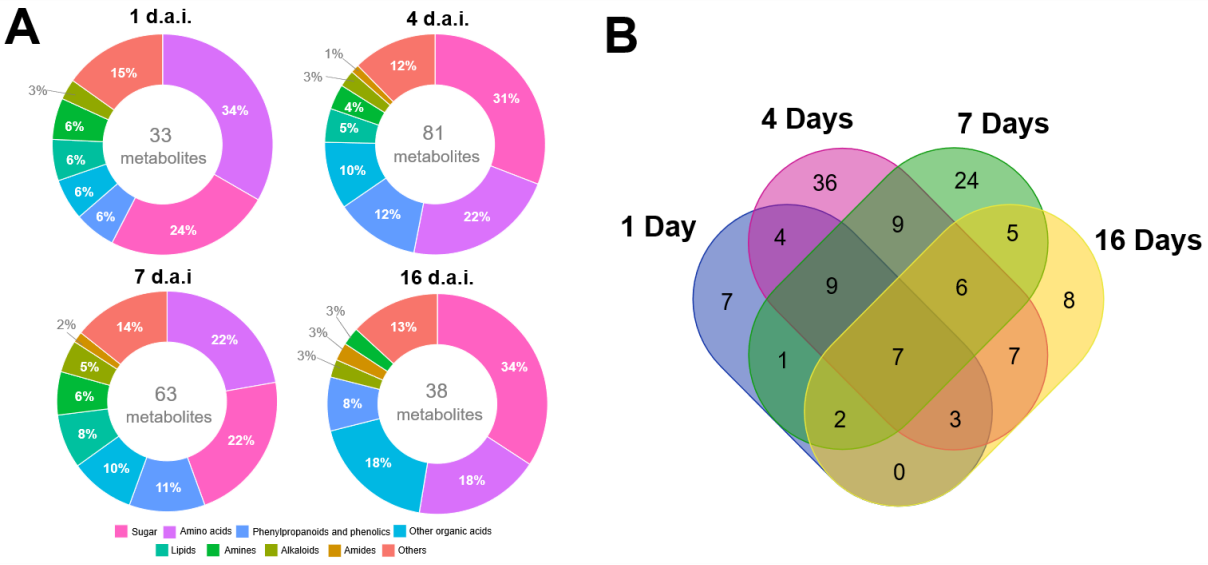


Figure 1. Metabolic class distribution and overlap of significantly altered polar metabolites during *Hemileia vastatrix* infection. (**A**) Pie charts showing the classification and number of metabolites showing statistically significant differences among control (C), resistant (R), and susceptible (S) Kawisari coffee hybrid leaf samples at 1, 4, 7, and 16 days after inoculation (DAI) with *H. vastatrix* (N = 5 biological replicates per treatment and time point). (**B**) Venn diagram illustrating the unique and shared differentially accumulated metabolites across the four post-inoculation time points.

Principal Component Analysis (PCA) was performed on the significantly different metabolites at each time point. This analysis revealed a clear separation among resistant, susceptible, and control samples, with the first two components explaining 70–80% of the total variance (Supplementary Figure S1). At the first time points (1, 4, and 7 DAI), resistant and susceptible samples were positioned on opposite sides of the first principal component, which accounted for around 50% of the variance. In contrast, 16 DAI, both inoculated groups (R and S) clustered together on one side of the first axis, opposite the control, with the first component explaining 65% of the variance (Supplementary Figure S1).

Pathway analysis (integrating metabolite set enrichment and pathway topology analysis, based on MetaboAnalyst) was performed for each time point (Figure 2). Among the significantly impacted metabolic pathways ($p \leq 0.05$ and impact > 0.2), *phenylalanine metabolism*, *arginine and proline metabolism*, and *phenylalanine, tyrosine* and *tryptophan biosynthesis* were consistently enriched at least three of the four time points studied, and collectively, these pathways highlighted the extensive modulation of amino acid metabolism throughout coffee-*H. vastatrix* interactions. In addition, the pathway associated with *starch and sucrose metabolism* was among the most impacted, exhibiting the highest enrichment at 4 DAI before declining. Pathways related to carbon fixation and central energy metabolism, including the *citrate cycle (TCA cycle)*, *carbon fixation by the Calvin cycle*, *pyruvate metabolism*, and *glyoxylate and dicarboxylate metabolism*, were predominantly enriched only at 16 DAI (Figure 2), indicating that perturbations in central carbon metabolism became more apparent at later stages of the interaction.

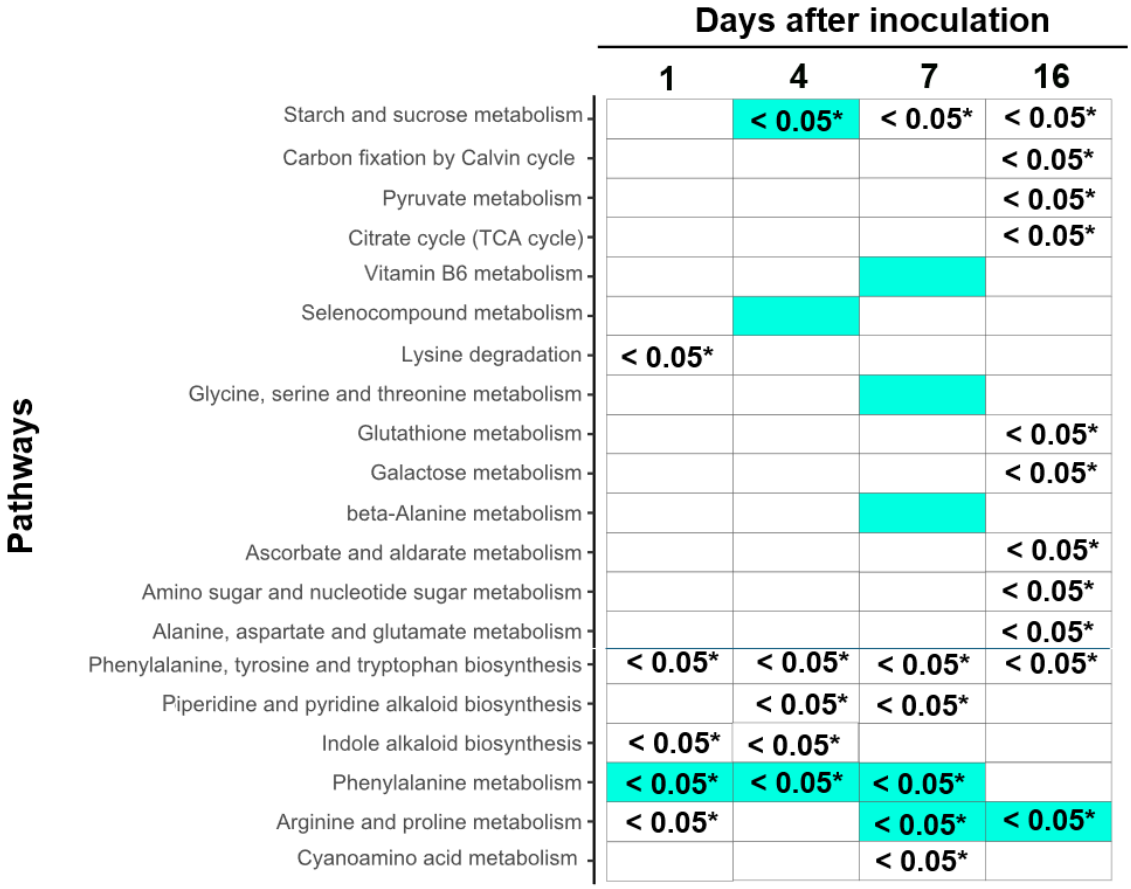


Figure 2. Metabolic pathway enrichment and topology analysis during coffee–*Hemileia vastatrix* interaction. Temporal representation of significantly impacted metabolic pathways identified via MetaboAnalyst 6.0 across post-inoculation time points (1, 4, 7, and 16 DAI) in Kawisari coffee leaves. Asterisks (*) denote statistically significant pathway enrichment (Fisher's exact test, $p < 0.05$). Highlighted cyan boxes indicate pathways with a pathway impact score > 0.2, calculated based on pathway topology analysis.

Focusing on the phenylpropanoid and phenolic classes (Figure 1A and Supplementary Table S2), KEGG pathway analysis revealed the enrichment of *flavonoid biosynthesis*, *phenylpropanoid biosynthesis*, *stilbenoid biosynthesis*, *tyrosine metabolism*, and *phenylalanine biosynthesis*, particularly at 4 and 7 DAI. L-Phenylalanine and, in some cases, L-tyrosine are the primary precursors of phenylpropanoid biosynthesis, originating from the shikimate

pathway. Both metabolites, along with their downstream phenolic derivatives, showed significant variation among the three samples at 4 and 7 DAI (Figure 3).

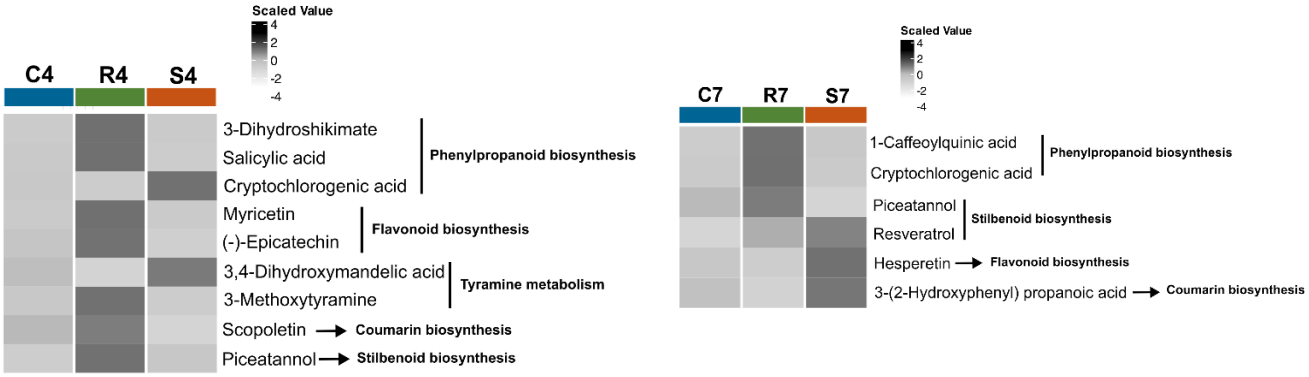


Figure 3. Accumulation patterns of key phenolic and phenylpropanoid metabolites at peak infection time points. Heatmaps showing the relative accumulation of differentially abundant metabolites within the phenylpropanoid, flavonoid, stilbenoid, coumarin, and tyramine biosynthetic pathways at 4 and 7 days after inoculation (DAI) with *Hemileia vastatrix*. Samples represent control (C), resistant (R), and susceptible (S) Kawisari leaf tissues ($N = 5$). Color gradients indicate scaled normalized metabolite peak intensities (Z-scores) from low (light gray) to high (dark gray/black).

In summary, pathway and metabolite-level analysis revealed dynamic and time-dependent enrichment patterns across multiple metabolic classes during the infection. Overall, these results indicate coordinated shifts in amino acid, carbohydrate, and phenylpropanoid metabolism, reflecting the dynamic nature of the coffee leaf response across the infection process.

3.2. Starch Quantification and Carbon Metabolism Enzymatic Activity Assays

Starch content (glucose equivalents) significantly increased in resistant Kawisari samples compared to both control and susceptible plants at 7 and 16 DAI (Figure 4A). Conversely, susceptible and control plants displayed lower starch levels at these late time points, with susceptible samples showing a marked decrease from days 7 to 16. To understand the metabolic pathways driving these distinct starch dynamics, we also analyzed the activities of the key enzymes involved in carbohydrate partitioning and mobilization by a semi-high-throughput analytical platform (Figure 4B). Heatmap analysis revealed that the most prominent enzymatic signature in resistant plants was a cluster comprising phosphoglucomutase (PGM), vacuolar invertase (vacInv), and cytosolic invertase (cytInv). These three enzymes exhibited a strong, coordinated increase in activity, specifically in the resistant samples at 7 and 16 DAI. This late enzymatic induction coincided with the massive accumulation of starch observed in the same samples (Figure 4A). This close correlation suggests that the simultaneous upregulation of PGM and PGI (at least at 7DAI) might facilitate the channelling of hexose-phosphates toward starch biosynthesis [56–58]. Concurrently, intracellular invertases (cytInv and vacInv) are co-activated at these late stages, indicating an intense turnover of soluble sugars alongside starch accumulation [59].

In contrast, a second, larger cluster comprised six of the nine analyzed enzymes (cwPOX, G6PDH, UGPase, PGI, cwInv, and Ald), which were characterized by higher relative activities in control and susceptible samples on the first day after inoculation (Figure 4B). Notably, the high initial activity of cell wall invertase (cwInv) in the 1 day control samples aligned with the low baseline starch levels observed at the beginning of the experiment, reflecting active carbon mobilization in these tissues prior to major metabolic reprogramming.

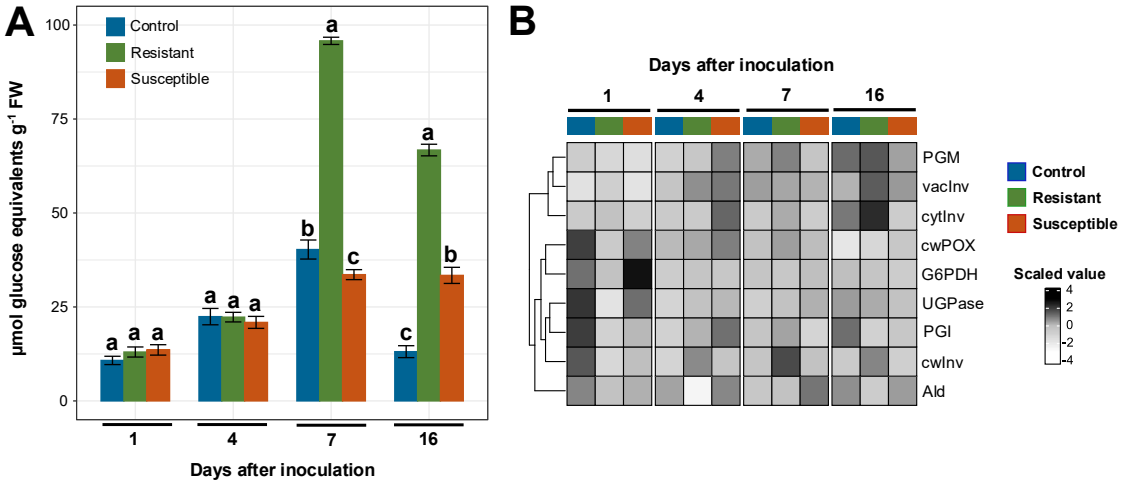


Figure 4. Starch accumulation dynamics and primary carbohydrate enzyme activity signatures. (**A**) Quantification of starch content (expressed as µmol glucose equivalents g^{-1} fresh weight) in Kawisari coffee leaves at 1, 4, 7, and 16 days after inoculation (d.a.i.) with *Hemileia vastatrix* across control (blue), resistant (green), and susceptible (orange) treatments. Bars represent mean values ±SD of five independent biological replicates ($N = 5$). Different lowercase letters above bars at a given time point indicate statistically significant differences determined by one-way ANOVA followed by Tukey's HSD post-hoc test ($p < 0.05$). (**B**) Hierarchical clustering heatmap of enzyme activity signatures normalized to total soluble protein (nkat · mg^{-1} protein). Rows represent individual enzymes, and columns display average activity per treatment across time points. Color scale ranges from lowest (white) to highest (dark gray/black) Z-score activity. *Enzyme abbreviations:* PGM, phosphoglucomutase; vacInv, vacuolar invertase; cytInv, cytoplasmic invertase; cwPOX, cell wall peroxidase; G6PDH, glucose-6-phosphate dehydrogenase; PGI, phosphoglucose isomerase; UGPase, UDP-glucose pyrophosphorylase; cwInv, cell wall invertase; and Ald, aldolase.

3.3. Gene Expression Analysis by RT-qPCR

To complement the metabolomic and enzymatic datasets and gain deeper insight into the regulatory mechanisms governing central carbon allocation, RT-qPCR analysis was performed on eight candidate genes previously identified through transcriptomic profiling [27]. These genes encode key enzymes at core metabolic junctions connecting central sugar partitioning, the pentose phosphate pathway (PPP), and downstream secondary metabolism. Overall, the greatest differences in gene expression between the resistant and susceptible samples were observed at 4 DAI (Figure 5). At this time point, *PPDK*, *S6PDH*, and *FBPase* expression was markedly repressed in resistant samples compared to susceptible samples. Conversely, *HPR* expression was strongly repressed in both samples, although the level of repression was significantly less pronounced in the resistant ones.

In contrast to this overall transcriptional suppression, *TK* and *RPE*, two key genes of the pentose phosphate pathway (PPP), were highly upregulated in resistant plants at 4 DAI. Although both samples (R and S) eventually reached their highest absolute expression levels for these two genes at 16 DAI, the striking differential upregulation at 4 DAI highlighted an early metabolic shift (Figure 5). This targeted activation of the PPP in resistant tissues likely serves to generate reducing power (NADPH) and essential biosynthetic precursors required to fuel downstream defense responses, such as reactive oxygen species (ROS) production and phenylpropanoid biosynthesis [22], the latter being consistent with the accumulated phenolics detected in the metabolomic data and described cytologically by Diniz et al. [26]. By 16 DAI, the transcriptional profiles of the resistant and

susceptible samples converged, showing no major differences in gene expression values, in accordance with the PCA results (Supplementary Figure S1).

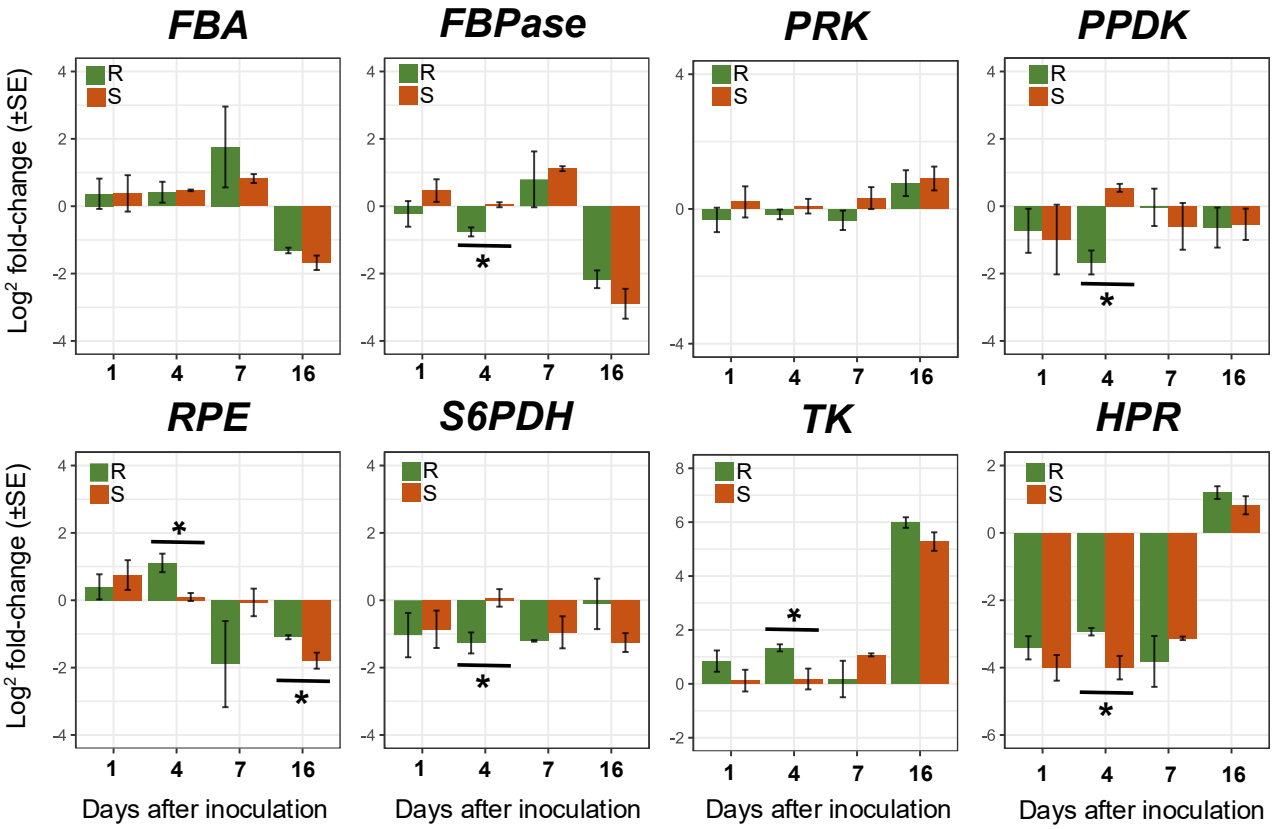


Figure 5. Gene expression analysis performed by RT-qPCR in the leaves of the Kawisari hybrid samples. Transcriptional profiles in resistant (R) and susceptible (S) leaves at 1, 4, 7, and 16 days after inoculation (DAI) with *Hemileia vastatrix*. Target genes were selected based on prior transcriptomic data [27] and encode key enzymes involved in central carbon metabolism, providing complementary transcriptional evidence for the observed metabolomic and enzymatic profiles. *Gene abbreviations*: *FBA*, fructose-bisphosphate aldolase; *FBPase*, cytosolic fructose-1,6-bisphosphatase; *PRK*, phosphoribulokinase; *PPDK*, cytosolic pyruvate, phosphate dikinase; *RPE*, ribulose-phosphate 3-epimerase; *S6PDH*, NADP-dependent D-sorbitol-6-phosphate dehydrogenase-like; *TK*, chloroplastic-like transketolase; *HPR*, hydroxypyruvate reductase. Each column represents the mean of three independent biological replicates, repeated at least three times, and error bars indicate standard error (±SD). Asterisks (*) represent statistical significance ($p < 0.05$) of gene expression differences between resistant and susceptible samples at each time point using Student's *t*-test.

3.4. Integrative Analysis

To gain a more comprehensive view of the coffee plant's response to *H. vastatrix*, a VIP score plot analysis (Figure 6 and Supplementary Table S3 [60]) was conducted by integrating data on primary metabolism-related metabolites (40 metabolites; Supplementary Table S4), gene expression, enzyme activity, and starch content of the coffee plants. This approach enabled the identification of the most influential variables contributing to coffee-*H. vastatrix* interactions. Metabolites such as L-asparagine, L-ornithine, spermine, 3- and hydroxypyruvic acid, along with specific enzymatic activities, including PGI, G6PDH, cytInv and cwPOX, appeared repeatedly across different time points with VIP scores > 1.5, highlighting their key roles in the metabolic response of coffee to *H. vastatrix*.

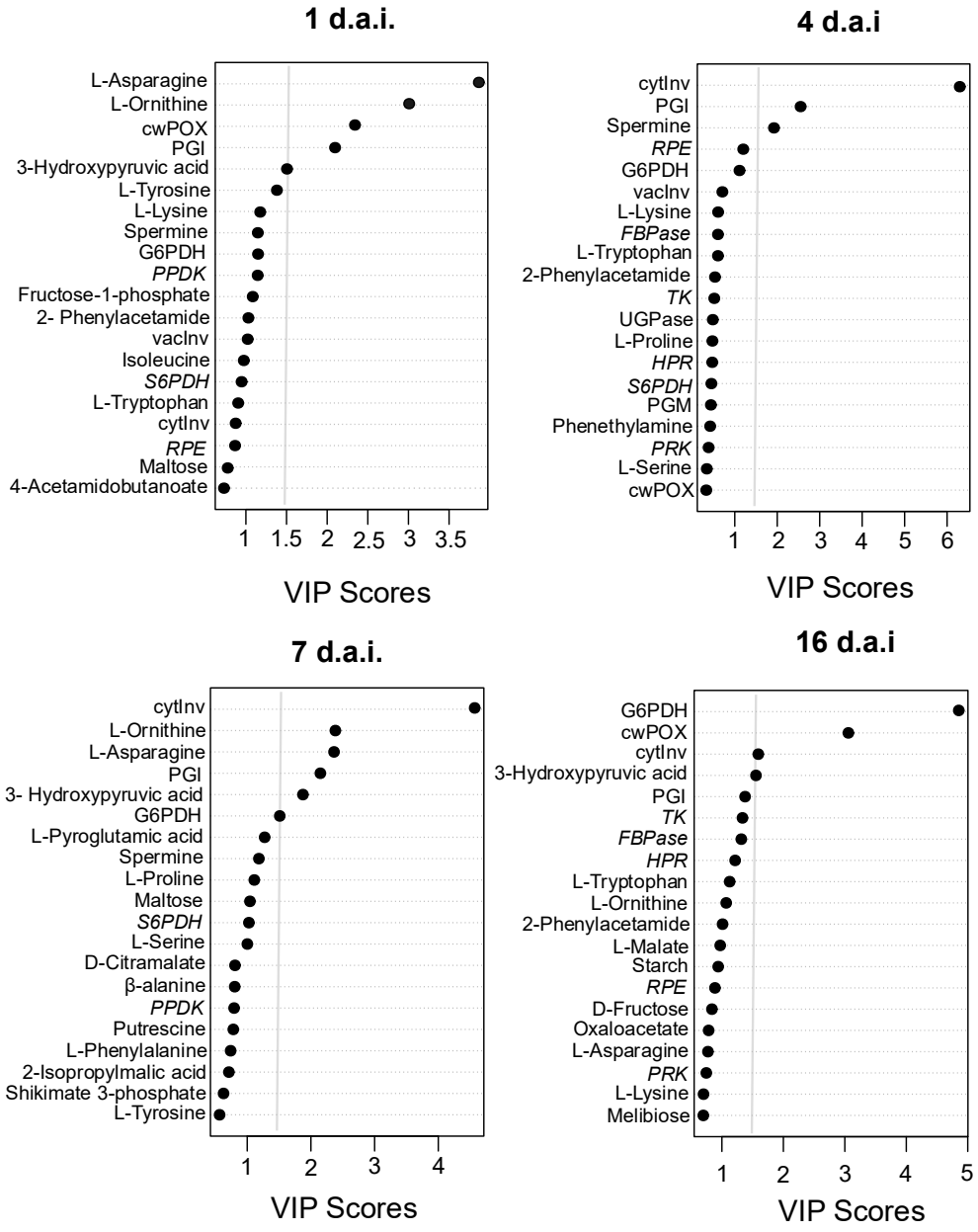


Figure 6. Multi-level data integration to identify candidate biomarkers using Partial Least Squares Discriminant Analysis (PLS-DA). Variable Importance in Projection (VIP) score plots derived from PLS-DA models integrating 40 primary metabolites, starch content, nine enzyme activity profiles, and eight target gene expression profiles across post-inoculation time points (1, 4, 7, and 16 d.a.i.). Variables with VIP scores > 1.0 (and particularly > 1.5) represent the main contributors to metabolic separation among control, resistant, and susceptible Kawisari leaves. *Nomenclature:* Gene names are presented in uppercase italics (*RPE*, *TK*, *FBPase*, *HPR*, *PPDK*, *S6PDH*), enzyme activity abbreviations are presented in regular font (e.g., PGI, G6PDH, cytInv, cwPOX), and metabolite names are presented in standard font, with initial capitalization.

4. Discussion

Unraveling the intricate biochemical mechanisms that govern plant immunity requires moving beyond descriptive pathways toward a systemic, multi-layered perspective. Accordingly, the integration of gene expression, enzymatic, starch, and metabolomic data through VIP score analysis (Figure 6) provided quantitative evidence that primary metabolism was actively restructured to drive the resistance of the Kawisari hybrid to *H.*

vastatrix. This coordinated metabolic reprogramming underscores that host defense is an energy-demanding process that requires a highly synchronized shift in carbohydrate partitioning and nitrogen allocation. By mapping these interactions, this study provides a comprehensive blueprint of how the early dynamics of primary metabolic networks are vital for fuelling and sustaining the downstream physiological barriers that arrest fungal colonization. This aligns with the general observation that carbohydrate metabolism and defence responses are coordinately regulated [16] with distinct differences observed in temporal dynamics between resistant and susceptible cultivars [61,62].

4.1. Carbon Allocation and Pentose Phosphate Pathway (PPP) Activation

The concurrent high ranking of PGI and PGM activities, together with the elevated expression of the chloroplastic-like *RPE* gene, supports the hypothesis of major metabolic reprogramming driving carbon diversion during *H. vastatrix* restriction. While PGI and PGM facilitate the mobilization and pooling of hexose-phosphates, upregulation of the RPE gene reflects an enhanced carbon flux through the PPP—a hallmark of plant immune responses. Activation of this pathway provides NADPH to sustain the plasma membrane NADPH oxidase-mediated oxidative burst, while recycling carbon skeletons for defense-related secondary metabolism. This metabolic commitment mirrors observations in the Arabidopsis–*Pseudomonas syringae* and wheat–*Puccinia striiformis* pathosystems, where genetic or enzymatic stimulation of the PPP is indispensable for sustained reactive oxygen species (ROS) production and the subsequent localized HR [19,57]. In previous studies on coffee–*H. vastatrix* interactions, increases in POX, ROS, and HR have been consistently associated with coffee resistance [1,63].

In parallel, the coordinated activation of PGI and PGM supports a unique pattern of carbon partitioning in the resistant response. Specifically, the significant accumulation of starch observed exclusively in the resistant Kawisari hybrid at 7 and 16 DAI indicates an active, defense-triggered carbon sequestration strategy. Starch accumulation has been reported during stress conditions when altered sink activity leads to marked shifts in carbon partitioning [64]. By shunting hexose-phosphates into transient starch reserves, the host effectively restricts the pool of free soluble sugars (such as sucrose and glucose) available in the apoplast and cytoplasm, depriving *H. vastatrix* of accessible nutrients during critical stages of post-haustorial colonization. In many biotrophic interactions, restricting free sugar availability induces fungal starvation, a mechanism tightly linked to sugar export inhibition and localized cell wall strengthening [59,65]. This nutrient restriction is particularly decisive because biotrophic pathogens, such as *H. vastatrix*, rely on hijacking host soluble sugars via upregulated transporters to establish susceptibility [23]. Rather than serving merely as a passive sink, this unique starch accumulation in the resistant interaction acts as a dynamic metabolic buffer. This strategic allocation allows carbon to be reserved and gradually redirected toward energy-demanding defense processes, such as the PPP and secondary metabolism (e.g., accumulation of phenolic-like compounds), while protecting primary metabolic functions from exhaustion. This plasticity is further reflected in sucrose dynamics: the simultaneous activation of intracellular invertases (cytInv and vacInv) in the Kawisari hybrid likely hydrolyzes cytosolic sucrose to fuel the PPP and phenolic synthesis without prematurely depleting the strategic starch reserves established at 7 and 16 DAI. Indeed, while cytosolic invertase and sucrose synthase generally handle basal sucrose turnover, the combined elevation of cytInv and vacInv ensures a continuous, tightly regulated hexose supply to sustain defense responses throughout the infection process [66].

4.2. The Primary-to-Secondary Metabolism Bridge for Phenolic Defense

Crucially, these adjustments in primary metabolic fluxes are intimately coupled with the activation of secondary defense lines, specifically phenylpropanoid and phenolic biosynthesis. The PPP does not merely supply NADPH for antioxidant management; it also provides erythrose-4-phosphate, which, together with glycolytic phosphoenolpyruvate, feeds the shikimate pathway [22]. This direct metabolic bridge explains the downstream accumulation of the aromatic amino acids L-phenylalanine and L-tyrosine and the subsequent enrichment of flavonoid, stilbenoid, and phenylpropanoid pathways observed at the critical early stages of infection (4 and 7 DAI). These results are in accordance with the increase in activity of the enzyme phenylalanine ammonia-liase along with the accumulation of phenolic-like compounds observed during coffee resistance, such as cell wall lignins and alkaloids [32]. A similar synchronized activation of the shikimate pathway and downstream phenylpropanoid metabolism has been extensively documented in resistant grapevine cultivars challenged with *Plasmopara viticola* and in rice defending against *Magnaporthe oryzae* [67,68]. The rapid accumulation of these phenolic metabolites (e.g., caffeoylquinic acid, chlorogenic acid, salicylic acid, epicatechin) in the Kawisari hybrid suggests their role as potent phytoanticipins and inducible phytoalexins, establishing a chemical barrier that directly impairs *H. vastatrix* haustoria differentiation and hyphal elongation within intercellular spaces. These findings align with previous cytological studies that observed the localized accumulation of phenolic compounds and haustorium encasement during the resistant response [26,27].

4.3. Nitrogen Remobilization and Polyamine-Mediated Signaling

In parallel to carbon reallocation, nitrogen metabolism undergoes profound restructuring during the resistant response, as highlighted by the high VIP scores of asparagine, ornithine, spermine, proline and serine. The accumulation of free amino acid pools is a well-known hallmark response in plants subjected to abiotic and biotic stresses [69]. This phenomenon is typically associated with controlled protein degradation, allowing the host to remobilize and "reinvest" amino acids into specialized pathways while adjusting growth-signaling events. Within this context, asparagine accumulation serves as a non-toxic, nitrogen-dense vehicle for resource remobilization when local primary metabolism is disrupted by pathogen invasion. This nitrogen-shuttling strategy is highly analogous to the metabolic responses observed in tomato leaves infected with *Botrytis cinerea* or *Cladosporium fulvum*, where host amino acid pools are dynamically shifted to preserve metabolic homeostasis [22].

Furthermore, ornithine is a critical metabolic hub that connects primary nitrogen assimilation to active chemical defense, serving as a direct precursor for both proline (involved in osmoprotection and ROS scavenging) and polyamines [70,71]. While asparagine reflects nitrogen remobilization to sustain the increased biosynthetic demand imposed by defense activation, ornithine likely supports polyamine biosynthesis [72]. This, in turn, provides substrates for H_2O_2 production through polyamine oxidation, thereby reinforcing the ROS-dependent defense response. Concurrently, changes in serine metabolism may further contribute to cellular redox homeostasis through one-carbon and sulfur pathways [21,73,74, 75].

In addition, the persistent identification of spermine and proline as top VIP features across multiple time points strongly supports the involvement of polyamines in Kawisari resistance. Polyamines are recognized not only as protective metabolites but also as crucial signaling players in host–pathogen crosstalk. Extracellular oxidation of spermine and spermidine by amine oxidases generates localized hydrogen peroxide (H_2O_2) contributing to the cell wall reinforcement matrix and triggering calcium-mediated defense signaling cascades. This polyamine-mediated defense deployment draws direct parallels to the

tobacco–*Tobacco Mosaic Virus* (TMV) interaction and the barley–*Blumeria graminis* pathosystem, where exogenous application or genetic overproduction of spermidine significantly enhanced resistance via the upregulation of pathogenesis-related (*PR*) genes and accelerated callose deposition [21,22,76].

Taken together, these multi-level data unveil a three-stage metabolic response associated with Kawisari hybrid resistance. An early (1–4 DAI) transcriptional activation of the pentose phosphate pathway (*RPE* and *TK*) is consistent with changes in primary metabolism and the potential generation of reducing power and precursors. This fuels the intermediate phase (4–7 DAI), characterized by the accumulation of phenolic defenses (caffeoylquinic acids, salicylic acid, flavonoids) alongside nitrogen remobilization (L-asparagine) and polyamine signaling (L-ornithine, spermine). Finally, a late-stage (7–16 DAI) shift in carbon partitioning, associated with elevated PGM and intracellular invertase activities, is accompanied by changes in starch content consistent with altered carbon allocation between soluble sugars and starch reserves. This reorganization may contribute to maintaining host energy balance and modulating nutrient availability during infection. Rather than acting in isolation, primary metabolic networks appear to coordinate early chemical barriers and late nutrient-limitation strategies against coffee rust.

5. Conclusions

This study provides insights into the primary metabolic processes associated with the defence of the Kawisari coffee hybrid against *H. vastatrix*. By applying a data integration approach, we identified a coordinated metabolic response involving three interconnected components. First, carbon partitioning was associated with the mobilization of starch reserves and changes in the pentose phosphate pathway, potentially supporting the provision of reducing power and precursors for phenolic metabolism. Second, nitrogen metabolism showed changes in amino acid profiles, including the accumulation of compounds involved in nitrogen transport, such as asparagine. Third, changes in polyamine profiles suggested a potential contribution of polyamine metabolism to the defence response. In addition to advancing our understanding of the metabolic responses associated with *Coffea* resistance, the identified enzyme activities, gene expression profiles, and metabolites represent potential biomarkers for further investigation. These candidates may be useful in future molecular breeding programs aimed at developing coffee varieties with improved and stable resistance to rust, supporting sustainable coffee production under climate and pathogen pressures.

Supplementary Materials: The following supporting information can be downloaded at: https://www.mdpi.com/article/10.3390/agronomy16212205/s1, Supplementary Table S1: List of primers used in the RT-qPCR analysis. Supplementary Table S2: List of the 215 metabolites identified through GC-TOF-MS non-targeted metabolomic analysis that exhibited statistically significant differences among the three Kawisari hybrid samples (control, resistant, and susceptible) at each time point, 1, 4, 7, and 16 days after inoculation with *H. vastatrix*. KEGG and HMDB_ID, KEGG_ID, KEGG_Pathway and Metabolic classes. Supplementary Figure S1: Principal Component Analysis (PCA) score plots of significantly altered leaf polar metabolites across infection stages. PCA score plots comparing control (C, blue), resistant (R, green), and susceptible (S, orange) Kawisari hybrid leaf samples at 1, 4, 7, and 16 days after inoculation (DAI) with *Hemileia vastatrix*. Data were log-transformed and mean-centered prior to analysis (N = 5 biological replicates). Colored shaded regions represent 95% confidence ellipses for each experimental group. The variance explained by PC1 and PC2 is indicated on each plot axis. Supplementary Table S3: Cross-validation (5-fold CV) performance metrics evaluated along the five components of the Partial Least Squares Discriminant Analysis (PLS-DA) model at 1, 4, 7, and 16 days after infection (DAI). Model performance parameters include accuracy, R2: coefficient of determination; Q2: predictive relevance based on the sum of

squared errors [60]. Supplementary Table S4: Variable Importance in Projection (VIP) score plot analysis from Partial Least Squares Discriminant Analysis (PLS-DA) integrating data of carbon metabolism (primary metabolites, gene expression, enzyme activities, and starch content). (*) The top 20 VIP values for the first principal component (Component 1) are highlighted in bold.

Author Contributions: L.G.-G. and C.P.: conceptualization; L.G.-G., M.d.C.S., C.P., J.C.D. and T.R.: design of the study; L.G.-G., H.G.A. and M.d.C.S.: biological material and inoculation; L.G.-G., J.C.C., J.C.D.: extraction and metabolomic analysis; L.G.-G., C.P., M.-E.-M.F. and T.R.: protein extraction and enzyme activity assays; L.G.-G., C.P. and J.C.C.: starch quantification; H.G.A., H.C. and M.D.F.: RNA extraction and RT-qPCR analysis; L.G.-G., C.P., H.G.A., J.C.D.: data analysis. L.G.-G. and H.G.A.: wrote the original draft of the manuscript. D.M.d.S.B.: references and first review of the manuscript. L.G.-G., M.d.C.S., J.C.D., C.P. and T.R.: funding acquisition. All authors contributed to manuscript revision, read, and approved the submitted version. All authors have read and agreed to the published version of the manuscript.

Funding: Funding of this work was provided by FCT—Fundação para a Ciência e a Tecnologia, I.P., through the project UID/04129/2025 (https://doi.org/10.54499/UID/04129/2025) of LEAF-Linking Landscape, Environment, Agriculture and Food Research Unit, the project LA/P/0092/2020 (DOI: 10.54499/LA/P/0092/2020) of the Associate Laboratory TERRA, and by FCT and FEDER funds (NORTE-01-0145-FEDER-029779 and LISBOA-01-0145-FEDER-029779) under the project CoffeeRES PTDC/ASP-PLA/29779/2017. This research was also supported by the project UIDP/04378/2020 (DOI: 10.54499/UIDP/04378/2020) and UIDB/04378/2020 (DOI: 10.54499/UIDB/04378/2020) of the Research Unit on Applied Molecular Biosciences—UCIBIO and the project LA/P/0140/2020 (DOI: 10.54499/LA/P/0140/2020) of the Associate Laboratory Institute for Health and Bioeconomy—i4HB, all funded by FCT I.P., Portugal. Financial support by the Access to Research Infrastructures activity in the Horizon2020 Program of the EU (EPPN2020 Grant Agreement 731013—ID524 and ID216) is gratefully acknowledged. J.C.C. was supported by the Brazilian agency Coordination for the Improvement of Higher Education Personnel (Coordenação de Aperfeiçoamento de Pessoal de Nível Superior—CAPES, funding code: 001).

Data Availability Statement: Metabolomics raw data, together with relevant metadata, is available at: Metabolights [77] and can be retrieved by searching for the manuscript title ("Multi-Level Data Integration Decodes the Metabolic Strategies of Kawisari Coffee Hybrid Resistance to *Hemileia vastatrix*") or upon request from the corresponding author. https://www.ebi.ac.uk/metabolights/ (accessed on 25 October 2026).

Acknowledgments: The Bachelor student Maria de Fátima Martins (NOVA-FCT) is acknowledged for her contribution to starch quantification.

Conflicts of Interest: The authors declare no conflicts of interest.

References

1. Silva, M.d.C.; Guerra-Guimarães, L.; Diniz, I.; Loureiro, A.; Azinheira, H.; Pereira, A.P.; Tavares, S.; Batista, D.; Várzea, V. An Overview of the Mechanisms Involved in Coffee-*Hemileia vastatrix* Interactions: Plant and Pathogen Perspectives. *Agronomy* **2022**, *12*, 326. https://doi.org/10.3390/agronomy12020326.
2. International Coffee Organization—ICO. COFFEE MARKET REPORTS—July 2026. Available online: https://www.ico.org/documents/cy2025-26/cmr-0726-e.pdf (accessed on 6 July 2026).
3. Talhinhas, P.; Batista, D.; Diniz, I.; Vieira, A.; Silva, D.N.; Loureiro, A.; Tavares, S.; Pereira, A.P.; Azinheira, H.G.; Guerra-Guimarães, L.; et al. Pathogen profile—The coffee leaf rust pathogen *Hemileia vastatrix*: One and a half centuries around the tropics. *Mol. Plant Pathol.* **2017**, *18*, 1039–1051. https://doi.org/10.1111/mpp.12512.
4. Lima, A.F.; dos Santos Botelho, D.M.; Guerra-Guimarães, L.; Andrade, V.T.; de Resende, M.L.V.; de Lima Santos, M.; de Rezende Abrahão, J.C. Evaluating coffee genotypes for resistance to coffee leaf rust in Brazil. *Trop. Plant Pathol.* **2025**, *50*, 2. https://doi.org/10.1007/s40858-024-00688-8.

5. Várzea, V.M.P.; Marques, D.V. Population variability of *Hemileia vastatrix* vs coffee durable resistance. In *Durable Resistance to Coffee Leaf Rust*; Zambolim, L., Zambolim, E., Várzea, V.M.P., Eds.; Universidade Federal de Viçosa: Viçosa, Brasil, 2005; pp. 53–74.
6. Bettencourt, A.J.; Rodrigues, C.J. Principles and practice of coffee breeding for resistance to rust and other diseases. In *Coffee Agronomy*; Clarke, R.J., Macrae, R., Eds.; Elsevier Applied Science Publishers LTD: London, UK; New York, NY, USA, 1988; Volume 4, pp. 199–234.
7. Barka, G.D.; Caixeta, E.T.; Ferreira, S.S.; Zambolim, L. In silico guided structural and functional analysis of genes with potential involvement in resistance to coffee leaf rust: A functional marker based approach. *PLoS ONE* **2020**, *15*, e0222747. https://doi.org/10.1371/journal.pone.0222747.
8. De Almeida, D.P.; Samila, I.; Castro, L.; Antônio, T.; Mendes, D.O.; Alves, D.R. Receptor-Like Kinase (RLK) as a candidate gene conferring resistance to *Hemileia vastatrix* in coffee. *Sci. Agric*. **2021**, *78*, e20200023. https://doi.org/10.1590/1678-992X-2020-0023.
9. Saavedra, L.M.; Caixeta, E.T.; Barka, G.D.; Borém, A.; Zambolim, L.; Nascimento, M.; Pereira, A.A. Marker-assisted recurrent selection for pyramiding leaf rust and coffee berry disease resistance alleles in *Coffea arabica* L. *Genes* **2023**, *14*, 189. https://doi.org/10.3390/genes14010189.
10. Prakash, N.S.; Marques, D.V.; Varzea, V.M.P.; Silva, M.C.; Combes, M.C.; Lashermes, P. Introgression molecular analysis of a leaf rust resistance gene from *Coffea liberica* into *C. arabica* L. *Theor. Appl. Genet*. **2004**, *109*, 1311–1317. https://doi.org/10.1007/s00122-004-1748-z.
11. Mengistu, M.W.; Workie, M.A.; Mohammed, A.S. Physical and Cup Quality Attributes of Arabica Coffee (*Coffea arabica* L.) Varieties Grown in Highlands of Amhara Region, Northwestern Ethiopia. *Int. J. Agron.* **2020**, 6420363. https://doi.org/10.1155/2020/6420363.
12. Lima, L.M.; de Pellegrini Elias, L.; e Silva, M.M.C.D.; da Silva, K.V.; Pacheco, A.S.V. Behavioral aspects of the coffee consumer in different countries: The case of Brazil. In *Coffee Consumption and Industry Strategies in Brazil 2020*; Woodhead Publishing: Cambridge, UK, 2020; pp. 321–341.
13. Reichel, T.; De Resende, M.L.V.; Nadaleti, D.H.S.; Santos, F.D.O.; Botelho, C.E. Potential of rust-resistant arabica coffee cultivars for specialty coffee production. *Biosci. J.* **2023**, *39*, e39055. https://doi.org/10.14393/BJ-v39n0a2023-66103.
14. Mahé, L.; Combes, M.C.; Várzea, V.M.P.; Guilhaumon, C.; Lashermes, P. Development of sequence characterized DNA markers linked to leaf rust (*Hemileia vastatrix*) resistance in coffee (*Coffea arabica* L.). *Mol. Breed*. **2008**, *21*, 105–113. https://doi.org/10.1007/s11032-007-9112-z.
15. Huang, X.; Bai, X.; Xie, Z.; Fahad, S.; Gbokie, T.; Lu, Y.; Guo, T.; Li, J.; Zhang, Z.; Wu, W.; et al. De novo transcriptome assembly of *Coffea liberica* reveals phylogeny and expression atlas of phenylalanine ammonia-lyase genes in *Coffea* species. *Ind. Crops Prod.* **2023**, *192*, 116029. https://doi.org/10.1016/j.indcrop.2022.116029.
16. Berger, S.; Sinha, A.K.; Roitsch, T. Plant Physiology meets phytopathology: Plant primary metabolism and plant-pathogen interactions. *J. Expt. Bot.* **2007**, *58*, 4019–4026. https://doi.org/10.1093/jxb/erm298.
17. Misra, V.; Mall, A.K.; Ansari, S.A.; Ansari, M.I. Sugar Transporters, Sugar-Metabolizing Enzymes, and Their Interaction with Phytohormones in Sugarcane. *J. Plant Growth Regul.* **2023**, *42*, 4975–4988. https://doi.org/10.1007/s00344-022-10778-z.
18. Zhang, Q.; Wang, Z.; Gao, R.; Jiang, Y. Sugars, Lipids and More: New Insights Into Plant Carbon Sources During Plant–Microbe Interactions. *Plant Cell Environ.* **2025**, *48*, 1656–1673. https://doi.org/10.1111/pce.15242.
19. Scharte, J.; Schön, H.; Tjaden, Z.; Weis, E.; von Schaewen, A. Isoenzyme replacement of glucose-6-phosphate dehydrogenase in the cytosol improves stress tolerance in plants. *Proc. Natl. Acad. Sci. USA* **2009**, *106*, 8061–8066. https://doi.org/10.1073/pnas.0812902106.
20. Maeda, H.; Dudareva, N. The Shikimate Pathway and Aromatic Amino Acid Biosynthesis in Plants. *Annu. Rev. Plant Biol.* **2012**, *63*, 73–105. https://doi.org/10.1146/annurev-arplant-042811-105439.
21. Walters, D. Resistance to plant pathogens: Possible roles for free polyamines and polyamine catabolism. *New Phytol.* **2003**, *159*, 109–115. https://doi.org/10.1046/j.1469-8137.2003.00802.x.
22. Seifi, H.S.; Shelp, B.J. Spermine Differentially Refines Plant Defense Responses Against Biotic and Abiotic Stresses. *Front. Plant Sci.* **2019**, *10*, 117. https://doi.org/10.3389/fpls.2019.00117.
23. Vieira, A.; Talhinhas, P.; Loureiro, A.; Thürich, J.; Duplessis, S.; Fernandez, D.; Silva, M.C.; Paulo, O.S.; Azinheira, H.G. Expression profiling of genes involved in the biotrophic colonisation of *Coffea arabica* leaves by *Hemileia vastatrix*. *Eur. J. Plant Pathol.* **2012**, *133*, 261–277. https://doi.org/10.1007/s10658-011-9864-5.

24. Possa, K.F.; Silva, J.A.G.; Resende, M.L.V.; Tenente, R.; Pinheiro, C.; Chaves, I.; Planchon, S.; Monteiro, A.C.A.; Renaut, J.; Carvalho, M.A.F.; et al. Primary metabolism is distinctly modulated by plant resistance inducers in *Coffea arabica* leaves infected by *Hemileia vastatrix*. *Front. Plant Sci.* **2020**, *11*, 309. https://doi.org/10.3389/fpls.2020.00309.
25. Guerra-Guimarães, L.; Diniz, I.; Azinheira, H.G.; Loureiro, A.; Pereira, A.P.; Tavares, S.; Batista, D.; Várzea, V.; Silva, M.D.C.L.D. Coffee Leaf Rust Resistance: An Overview. In *Mutation Breeding in Coffee with Special Reference to Leaf Rust*; Ingelbrecht, I.L., Silva, M.d.C., Jankowicz-Cieslak, J., Eds.; Springer: Berlin, Heidelberg, 2023; pp 19–38. https://doi.org/10.1007/978-3-662-67273-0_2.
26. Diniz, I.; Figueiredo, A.; Sebastiana, M.; Munoz-Pajarez, A.J.; Valverde, J.; Azevedo, H.; Rodrigues, A.S.; Prakash, R.S.; Pereira, A.P.; Guerra-Guimarães, L.; et al. First steps on the resistance profiling of Kawisari coffee hybrid through cytological and gene expression analyses. In Proceedings of the 28th International Conference on Coffee Science (ASIC), Montpellier, France, 28 June–1 July 2021; p. 60.
27. Azevedo, H.; Diniz, I.; Figueiredo, A.; Guedes, F.A.F.; Sebastiana, M.G.; Azinheira, H.G.; Barros, D.; Castro, P.H.; Loureiro, A.; Muñoz-Pajares, A.J.; et al. Characterization of the transcriptional signatures associated with resistance and susceptibility to *Hemileia vastatrix* in the Kawisari coffee hybrid. In Proceedings of the Translational Research in Crops, Ghent, Belgium, 22–23 June 2023. Available online: http://hdl.handle.net/10400.5/28027 (accessed on 8 August 2023).
28. Huot, B.; Yao, J.; Montgomery, B.L.; He, S.Y. Growth–defense trade-offs in plants: A balancing act to survive in a dynamic environment. *Mol. Plant* **2014**, *7*, 1267–1287. https://doi.org/10.1093/mp/ssu049.
29. Zandalinas, S.I.; Fritschi, F.B.; Mittler, R. Global warming, climate change, and environmental pollution: Recipe for a multifactorial stress combination disaster. *Trends Plant Sci.* **2021**, *26*, 588–599. https://doi.org/10.1016/j.tplants.2021.02.011.
30. DaMatta, F.M.; Martins, S.C.V.; Ramalho, J.C. Ecophysiology of coffee growth and production in a context of climate changes. In *Advances in Botanical Research*; Chapter 4; Academic Press: Cambridge, MA, USA, 2025; Volume 114, pp. 97–139. https://doi.org/10.1016/bs.abr.2024.07.004.
31. Jammer, A.; Akhtar, S.S.; Buchvaldt Amby, D.; Pandey, C.; Mekureyaw, M.F.; Bak, F.; Roitsch, T. Enzyme activity profiling as an emerging tool for cell physiological phenotyping within functional phenomics to assess plant growth and stress responses. *J. Exp. Bot.* **2022**, *73*, 5170–5198. https://doi.org/10.1093/jxb/erac215.
32. Silva, M.C.; Nicole, M.; Guerra-Guimarães, L.; Rodrigues, C.J., Jr. Hypersensitive cell death and post-haustorial defence responses arrest the orange rust (*Hemileia vastatrix*) growth in resistant coffee leaves. *Physiol. Mol. Plant Pathol.* **2002**, *60*, 169–183. https://doi.org/10.1006/pmpp.2002.0389.
33. Salem, M.A.; Perez de Souza, L.; Serag, A.; Fernie, A.R.; Farag, M.A.; Ezzat, S.M.; Alseekh, S. Metabolomics in the Context of Plant Natural Products Research: From Sample Preparation to Metabolite Analysis. *Metabolites* **2020**, *10*, 37. https://doi.org/10.3390/metabo10010037.
34. Carréra, J.C.; Guerra-Guimarães, L.; D'Auria, J.C.; de Jesus Sartori, L.; Pinheiro, C.; Silva, V.A.; Volpato, M.L.; Carvalho, G.R.; Mori, F.A. Non-targeted metabolomic analysis of field-grown *Coffea arabica* cultivars reveals distinct leaf metabolic signatures. *Theor. Exp. Plant Physiol.* **2025**, *37*, 27. https://doi.org/10.1007/s40626-025-00373-4.
35. Hummel, J.; Strehmel, N.; Bölling, C.; Schmidt, S.; Walther, D.; Kopka, J. Mass Spectral Search and Analysis Using the Golm Metabolome Database. In *The Handbook of Plant Metabolomics*; Weckwerth, W., Kahl, G., Eds.; 2013. https://doi.org/10.1002/9783527669882.ch18.
36. Kanehisa, M.; Furumichi, M.; Sato, Y.; Kawashima, M.; Ishiguro-Watanabe, M. KEGG for taxonomy-based analysis of pathways and genomes. *Nucleic Acids Res.* **2023**, *51*, D587–D592. https://doi.org/10.1093/nar/gkac963.
37. Wishart, D.S.; Guo, A.; Oler, E.; Wang, F.; Anjum, A.; Peters, H.; Dizon, R.; Sayeeda, Z.; Tian, S.; Lee, B.L.; et al. HMDB 5.0: The human metabolome database for 2022. *Nucleic Acids Res.* **2022**, *50*, D622–D631. https://doi.org/10.1093/nar/gkab1062.
38. Pinheiro, C.; Emiliani, G.; Marino, G.; Fortunato, A.S.; Haworth, M.; De Carlo, A.; Chaves, M.M.; Loreto, F.; Centritto, M. Metabolic Background, Not Photosynthetic Physiology, Determines Drought and Drought Recovery Responses in C3 and C2 Moricandias. *Int. J. Mol. Sci.* **2023**, *24*, 4094. https://doi.org/10.3390/ijms24044094.
39. Jammer, A.; Gasperl, A.; Luschin-Ebengreuth, N.; Heyneke, E.; Chu, H.; Cantero-Navarro, E.; Großkinsky, D.K.; Albacete, A.A.; Stabentheiner, E.; Franzaring, J.; et al. Simple and robust determination of the activity signature of key carbohydrate metabolism enzymes for physiological phenotyping in model and crop plants. *J. Exp. Bot.* **2015**, *66*, 5531–5542. https://doi.org/10.1093/jxb/erv228.
40. Fimognari, L.; Dölker, R.; Kaselyte, G.; Jensen, C.N.; Akhtar, S.S.; Großkinsky, D.K.; Roitsch, T. Simple semi-high throughput determination of activity signatures of key antioxidant enzymes for physiological phenotyping. *Plant Methods* **2020**, *16*, 42. https://doi.org/10.1186/s13007-020-00583-8.

41. Bradford, M.M. A rapid and sensitive method for quantification of microgram quantities of protein utilizing the principle of protein-dye binding. *Anal. Biochem.* **1976**, *72*, 248–254.
42. Tavares, S.; Azinheira, H.; Valverde, J.; Muñoz-Pajares, A.J.; Talhinhas, P.; Silva, M.d.C. Identification of HIR, EDS1 and PAD4 Genes Reveals Differences between *Coffea* Species That May Impact Disease Resistance. *Agronomy* **2023**, *13*, 992. https://doi.org/10.3390/agronomy13040992.
43. Fiehn, O. Metabolomics by Gas Chromatography–Mass Spectrometry: Combined Targeted and Untargeted Profiling. *Curr. Protoc. Mol. Biol.* **2016**, *114*, 21.33.1–21.33.11. https://doi.org/10.1002/0471142727.mb3004s114.
44. Fiehn, O.; Wohlgemuth, G.; Scholz, M.; Kind, T.; Lee, D.Y.; Lu, Y.; Moon, S.; Nikolau, B. Quality control public databases for GC-MS-based untargeted metabolomics. *Plant J.* **2008**, *53*, 691–704. https://doi.org/10.1111/j.1365-313X.2007.03387.x.
45. RCoreTeam R: A Language and Environment for Statistical Computing. Version 4.3.1. R Foundation for Statistical Computing, Vienna, Austria, 2023. Available online: https://www.R-project.org/ (accessed on 27 October 2023).
46. Pang, Z.; Lu, Y.; Zhou, G.; Hui, F.; Xu, L.; Viau, C.; Spigelman, A.F.; MacDonald, P.E.; Wishart, D.S.; Li, S.; et al. MetaboAnalyst 6.0: Towards a unified platform for metabolomics data processing, analysis and interpretation. *Nucleic Acids Res.* **2024**, *52*, W398–W406. https://doi.org/10.1093/nar/gkae253.
47. Gu, Z.; Gu, L.; Eils, R.; Schlesner, M.; Brors, B. *Circlize* implements and enhances circular visualization in R. *Bioinformatics* **2014**, *30*, 2811–2812, https://doi.org/10.1093/bioinformatics/btu393.
48. Gu, Z.; Eils, R.; Schlesner, M. Complex heatmaps reveal patterns and correlations in multidimensional genomic data. *Bioinformatics* **2016**, *32*, 2847–2849. https://doi.org/10.1093/bioinformatics/btw313.
49. Gu, Z. Complex heatmap visualization. *iMeta* **2022**, *1*, e43. https://doi.org/10.1002/imt2.43.
50. Wickham, H.; François, R.; Henry, L.; Müller, K.; Vaughan, D. *dplyr: A Grammar of Data Manipulation.* R package version 1.2.1, 2023. Available online: https://dplyr.tidyverse.org (accessed on 8 September 2026).
51. Wickham, H. Programming with ggplot2. In *Ggplot2: Elegant Graphics for Data Analysis*; Springer International Publishing: Cham, Switzerland, 2016; pp. 241–253.
52. Rinker, T.W.; Kurkiewicz, D. pacman: Package management for R. version 0.5. 0. Buffalo, New York, 2017. Available online: http://github.com/trinker/pacman (accessed on 9 September 2025).
53. Fox, J.; Weisberg, S. *An R Companion to Applied Regression*, 3rd ed.; Sage: Thousand Oaks CA, USA, 2019. Available online: http://z.umn.edu/carbook (accessed on 30 April 2025).
54. Herve, M. *RVAideMemoire: Testing and Plotting Procedures for Biostatistics*. R package version 0.9-83-12, 2025. Available online: https://CRAN.R-project.org/package=RVAideMemoire (accessed on 30 April 2025).
55. Greenwell, B.M.; Boehmke, B.C. Variable Importance Plots—An Introduction to the vip Package. *R. J.* **2020**, *12*, 343–366. https://doi.org/10.32614/RJ-2020-013.
56. Bahaji, A.; Sánchez-López, Á.M.; De Diego, N.; Muñoz, F.J.; Baroja-Fernández, E.; Li, J.; Pozueta-Romero, J. Plastidic phosphoglucose isomerase is an important determinant of starch accumulation in *Arabidopsis thaliana* leaves. *J. Exp. Bot.* **2014**, *65*, 4627–4639. https://doi.org/10.1093/jxb/eru225.
57. Streb, S.; Zeeman, S.C. Starch metabolism in *Arabidopsis*. *Arab. Book.* **2012**, *10*, e0160. https://doi.org/10.1199/tab.0160.
58. Kanwar, P.; Jha, G. Alterations in plant sugar metabolism: Signatory of pathogen attack. *Planta* **2019**, *249*, 305–318. https://doi.org/10.1007/s00425-018-3018-3.
59. Ruan, Y.-L. Sucrose metabolism: Gateway to diverse carbon use and sugar signaling. *Annu. Rev. Plant Biol.* **2014**, *65*, 33–67. https://doi.org/10.1146/annurev-arplant-050213-040251.
60. Szymańska, E.; Saccenti, E.; Smilde, A. K.; Westerhuis, J. A. Double-check: validation of diagnostic statistics for PLS-DA models in metabolomics studies. *Metabolomics* **2012**, 8, 3–16. https://doi.org/10.1007/s11306-011-0330-3.
61. Pandey, C.; Großkinsky, D.K.; Westergaard, J.C.; Jørgensen, H.J.L.; Svensgaard, J.; Christensen, S.; Schulz, A.; Roitsch, T. Identification of a bio-signature for barley resistance against *Pyrenophora teres* infection based on physiological, molecular and sensor-based phenotyping. *Plant Sci.* **2021**, *313*, 111072. https://doi.org/10.1016/j.plantsci.2021.111072.
62. Vega-Álvarez, C.; Soengas, P.; Roitsch, T.; Abilleira, R.; Velasco, P.; Francisco, M. Unveiling plant defense arsenal: Metabolic strategies in Brassica oleracea during black rot disease. *Hortic. Res.* **2023**, *10*, uhad204. https://doi.org/10.1093/hr/uhad204.
63. Silva, M.C.; Guerra-Guimarães, L.; Loureiro, A.; Nicole, M.R. Involvement of peroxidases in the coffee resistance to orange rust *(Hemileia vastatrix). Physiol. Mol. Plant Pathol.* **2008**, *72*, 29–38. https://doi.org/10.1016/j.pmpp.2008.04.004.
64. Chaves, M.M.; Flexas, J.; Pinheiro, C. Photosynthesis under drought and salt stress—Regulation mechanisms from whole plant to cell. *Ann. Bot.* **2009**, *103*, 551–560. https://doi.org/10.1093/aob/mcn125.

65. Tauzin, A.S.; Giardina, T. Sucrose and invertases, a part of the plant defense response to the biotic stresses. *Front. Plant Sci.* **2014**, *5*, 293. https://doi.org/10.3389/fpls.2014.00293.
66. Roitsch, T.; González, M.C. Function and regulation of plant invertases: Sweet sensations. *Trends Plant Sci.* **2004**, *9*, 606–613. https://doi.org/10.1016/j.tplants.2004.10.009.
67. Figueiredo, A.; Fortes, A.M.; Ferreira, S.; Sebastiana, M.; Choi, Y.H.; Sousa, L.; Acioli-Santos, B.; Pessoa, F.; Verpoorte, R.; Pais, M.S. Transcriptional and metabolic profiling of grape (*Vitis vinifera* L.) leaves unravel possible innate resistance against pathogenic fungi. *J. Exp. Botany* **2008**, *59*, 3371–3381, https://doi.org/10.1093/jxb/ern187.
68. Duan, L.; Liu, H.; Li, X.; Xiao, J.; Wang, S. Multiple phytohormones and phytoalexins are involved in disease resistance to *Magnaporthe oryzae* invaded from roots in rice. *Physiol. Plant.* **2014**, *152*, 486–500. https://doi.org/10.1111/ppl.12192.
69. Alves, M.; Chicau, P.; Matias, H.; Passarinho, J.; Pinheiro, C.; Ricardo, C.P. Metabolic analysis revealed altered amino acid profiles in *Lupinus albus* organs as a result of boron deficiency. *Physiol. Plant.* **2011**, *142*, 224–232 https://doi.org/10.1111/j.1399-3054.2011.01462.x.
70. He, M.; He, C.-Q.; Ding, N.-Z. Abiotic Stresses: General Defenses of Land Plants and Chances for Engineering Multistress Tolerance. *Front. Plant Sci.* **2018**, *9*, 1771. https://doi.org/10.3389/fpls.2018.01771.
71. Winter, G.; Todd, C.D.; Trovato, M.; Forlani, G.; Funck, D. Physiological implications of arginine metabolism in plants. *Front. Plant Sci.* **2015**, *6*, 534. https://doi.org/10.3389/fpls.2015.00534.
72. Qiao, G.; Xiao, S.; Dong, J.; Yang, Q.; Che, H.; Sun, X. The Multifaceted Functions of Plant Asparagine Synthetase: Regulatory Mechanisms and Functional Diversity in Growth and Defense. *Plants* **2026**, *15*, 362. https://doi.org/10.3390/plants15030362.
73. Yu, Y.; Zhou, W.; Zhou, K.; Liu, W.; Liang, X.; Chen, Y.; Sun, D.; Lin, X. Polyamines modulate aluminum-induced oxidative stress differently by inducing or reducing H2O2 production in wheat. *Chemosphere* **2018**, *212*, 645–653. https://doi.org/10.1016/j.chemosphere.2018.08.133.
74. Ros, R.; Muñoz-Bertomeu, J.; Krueger, S. Serine in plants: Biosynthesis, metabolism, and functions. *Trends Plant Sci.* **2014**, *19*, 564–569. https://doi.org/10.1016/j.tplants.2014.06.003.
75. Zimmermann, S.E.; Benstein, R.M.; Flores-Tornero, M.; Blau, S.; Anoman, A.D.; Rosa-Téllez, S.; Gerlich, S.C.; Salem, M.A.; Alseekh, S.; Kopriva, S.; et al. The phosphorylated pathway of serine biosynthesis links plant growth with nitrogen metabolism. *Plant Physiol.* **2021**, *186*, 1487–1506, https://doi.org/10.1093/plphys/kiab167.
76. Ross, W.F.; Walters, D.R.; Robins, D.J. Synthesis and antifungal activity of five classes of diamines. *Pest. Manag. Sci.* **2004**, *60*, 143–148. https://doi.org/10.1002/ps.794.
77. Haug, K.; Cochrane, K.; Nainala, V.C.; Williams, M.; Chang, J.; Jayaseelan, K.V.; O'Donovan, C. MetaboLights: A resource evolving in response to the needs of its scientific community. *Nucleic Acids Res.* **2020**, *48*, D440–D444, https://doi.org/10.1093/nar/gkz1019.

Disclaimer/Publisher's Note: The statements, opinions and data contained in all publications are solely those of the individual author(s) and contributor(s) and not of MDPI and/or the editor(s). MDPI and/or the editor(s) disclaim responsibility for any injury to people or property resulting from any ideas, methods, instructions or products referred to in the content.